Molecular Dynamics Simulations of the Dielectric Constants of Salt-Free and Salt-Doped Polar Solvents

Cameron J. Shock¹, Mark J. Stevens², Amalie L. Frischknecht²*, and Issei Nakamura¹*

¹Department of Physics, Michigan Technological University, Houghton, Michigan 49931, United States

²Center for Integrated Nanotechnologies, Sandia National Laboratories, Albuquerque, New Mexico 87185, United States

*alfrisc@sandia.gov, *inakamur@mtu.edu

We develop a Stockmayer fluid model that accounts for the dielectric responses of polar solvents (water, MeOH, EtOH, acetone, 1-propanol, DMSO, and DMF) and NaCl solutions. These solvent molecules are represented by Lennard–Jones spheres with permanent dipole moments and the ions by charged Lennard-Jones spheres. The simulated dielectric constants of these liquids are comparable to experimental values, including the substantial decrease in the dielectric constant of water upon the addition of NaCl. Moreover, the simulations predict an increase in the dielectric constant when considering the influence of ion translations in addition to the orientation of permanent dipoles.

I. INTRODUCTION

Understanding the dielectric responses of polar liquids at the atomic and molecular level is of paramount importance in soft matter science. Computational modeling of electric polarization is a rapidly developing subject that has been particularly accelerated by recent innovations in computer hardware and infrastructure and advancements in machine learning algorithms. Accordingly, numerous force-field models for atomistic molecular dynamics (MD) simulations have been developed to investigate the dielectric response of saltfree and salt-doped water. 1-8 Nevertheless, development of versatile simulation methods that simultaneously account for the dielectric responses of various polar liquids is challenging because simulation results are typically sensitive to multiple model parameters and the surrounding conditions. The reproduction of the observed dielectric values in computer simulations typically requires careful tuning of the model parameters, including the electronic polarizability, dipole moment, particle diameter, and dispersion forces, while maintaining model robustness against changes in environmental parameters such as the temperature, mixing ratio, and density. Moreover, the difficulty in validating the model and the computational feasibility of considering diverse types of polar liquids substantially increase when salt ions or liquid mixtures are involved.9-14

This work focuses on calculating the static dielectric constants of salt-free polar liquids and NaCl solutions. Determining the dielectric constant of polar liquids is important for understanding the mechanisms underlying ion solvation, 15, 16 charge transport, 17, 18 and other material thermodynamic properties.¹⁹ Various methods can be applied to calculate these quantities with varying degrees of success. The Kirkwood-Fröhlich theory introduces a multiplicative correlation factor (g-factor) for an orientational correlation function that accounts for the significant effect of hydrogen bonding on the dielectric constant.²⁰ While the g-factor for water molecules can be analytically calculated at the meanfield level, in practice, this quantity is often invoked as a fitting parameter to better match the theory with the experimentally determined value.²¹ Regardless, the Kirkwood-Fröhlich equation (or its variants, such as the Booth equation²²) tends to be qualitatively and quantitatively consistent with the experimental data for the dielectric constants of various polar liquids. However, simulation models, even those with multiple model parameters, are often outperformed by Kirkwood-Fröhlich theory-class equations,²³ and this undesirable situation needs to be qualitatively understood in soft matter science, in which a broad spectrum of ions and molecules tend to be simultaneously involved and strongly correlated. Thus, this article aims to develop a Stockmayer fluid (SF) model that accounts for experimental observations,

including the effects caused by salt ions dissolved in water.

The SF model is a simple coarse-grained model consisting of Lennard-Jones spheres with permanent dipole moments that has a faster computation time than atomistic models while maintaining the major influences on the dielectric nature of these materials. Due to the simplicity of the model and its compatibility theoretical techniques in thermodynamics, the SF model has been employed to study liquid-vapor phase coexistence and critical behavior, as well as the thermodynamic and dynamical properties of polar fluids.²⁴⁻²⁸ Moreover, the SF model has been applied to simulations to investigate phase coexistence²⁹⁻³⁴ and the dielectric responses^{14, 35} of polar liquids and has successfully qualitatively predicted the nature of the solvation energies of various solvents and ions³⁶ and the dielectric constants of ellipsoidal organic solvents.³⁷ Despite its increasing use and success, many questions remain about the model's viability for predicting important properties such as the dielectric constant, viscosity, and ionic conductivity. Specifically, the application of the SF model to ion-containing fluids³⁸ is significantly limited in both the theory and simulation literature.

The remainder of this paper is organized as follows. First, we consider the SF model as a computationally fast and adaptable model (Section II) and discuss that the dipole moment in the simulation input should fall in the range between the scaled dipole moment and effective dipole moment in the liquid phase (Section IIA). The dielectric constant calculation for electrolytes in the literature often ignores the contribution of collective ion translational motion.^{39, 40} This effect can be evaluated by the Einstein-Helfand (EH) method^{40, 41} (Section IIB). The simulation results are presented in Section III. In our simulation methodology, the model parameters may not be uniquely determined or may be slightly altered to approximate the experimental data. This paradigm allows our SF MD model to be more versatile than atomistic simulations. Thus, we provide multiple sets of model parameters in Table 1. Readers interested in further methodology for optimizing the model parameters in SF models should refer to Ref. 42 which describes the use of ensemble neural network methods for parameter optimization.

We also discuss the temperature dependence of the dielectric constant of salt-free water. In addition, we show that the dielectric constants of NaCl solutions decrease as the salt concentration increases. This dielectric decrement arises primarily from saturated dipoles near the salt ions but appears to be mitigated when charge-neutral ion pairs are formed. Moreover,

our results predict that including ion translational motion leads to a monotonic increase in the dielectric constant.

II. COMPUTATIONAL METHOD A. Molecular Dynamics Simulation

Our simulation strategy involves developing a coarse-grained model that treats charge-neutral polar molecules as spheres with a diameter of σ and a freely rotating permanent dipole with dipole moment $\vec{\mu}$. The excluded volume potential is given by the Lennard-Jones (LJ) potential,

$$\begin{cases} U_{LJ} = 4\epsilon_{LJ} \left[\left(\frac{\sigma}{r} \right)^{12} - \left(\frac{\sigma}{r} \right)^{6} \right] & (r \le r_c) \\ U_{LJ} = 0 & (r > r_c) \end{cases}$$
 Eq. 1

where $\epsilon_{\rm LJ}$ and $r=|r_i-r_j|$ designate the potential well depth and the distance between particles i and j, respectively. In this work we use the modification to the LJ potential known as the Weeks-Chandler-Andersen (WCA) potential, which has a cutoff of $r_c=2^{\frac{1}{6}\sigma}$ that yields a purely repulsive potential. Geometric mixing rules are often assumed for the interaction parameters between dissimilar species i and j, namely, $\epsilon_{\rm LJ}^{(i,j)}=$

 $\sqrt{\epsilon_{LJ}^{(i,i)} \cdot \epsilon_{LJ}^{(j,j)}}$ and $\sigma^{(i,j)} = \sqrt{\sigma^{(i,i)} \cdot \sigma^{(j,j)}}$. We also follow these rules for the solvents; however, we independently change $\epsilon_{LJ}^{(i,j)}$ in the case of salt-doped solvents to prevent tightly bound ion clusters.

The effect of the induced dipole moment can also be accounted for by considering the attractive part in the LJ potential, because the thermodynamic average of the induced dipole-dipole interaction is proportional to $-1/r^6$, which is often called the Keesom potential. We consider this effect in the sections involving temperature dependence with an NPT ensemble, external electric fields, and salt solutions, otherwise this is not used in the case of the WCA potential. The present treatment with the WCA potential is consistent with that in our previous work on the solvation energy of ions dissolved in polar solvents, where dipolar interactions come only from the fixed dipoles and not from the attractive part of the LJ interaction, i.e. the polarization is considered using effective dipoles.³⁶ Accordingly, we formulate the dipole–dipole interaction between the ith and *j*th particles as

$$U_{\mu\mu} = \frac{1}{4\pi\varepsilon_0} \left[\frac{\left(\overrightarrow{\mu_l} \cdot \overrightarrow{\mu_j} \right)}{r^3} - \left(\frac{3}{r^5} \right) (\overrightarrow{\mu_l} \cdot \overrightarrow{r}) \left(\overrightarrow{\mu_j} \cdot \overrightarrow{r} \right) \right]. \quad \text{Eq. 2}$$

For salt-doped solvents, the charge-dipole interaction between the ion and the solvent at a distance of r is:

$$U_{q\mu} = \frac{q(\vec{\mu} \cdot \vec{r})}{4\pi\varepsilon_0 r^3},$$
 Eq. 3

where q designates the ionic charge. The ion-ion interaction between charges q_i and q_j is given by the standard Coulomb form,

$$U_{qq} = \frac{q_i q_j}{4\pi\varepsilon_0 r}$$
. Eq. 4

In atomistic simulations it is common to use a charge scaling scheme in which the electric charge q in a molecule is reduced to $\approx q/\sqrt{\varepsilon_{\infty}}$ (or $\frac{q}{n}$ when $\varepsilon_{\infty}=n^2$) with a high-frequency dielectric constant (or refractive index n) in order to account for charge screening due to electronic polarization. 12, 43-47 In the present case with a coarse-grained SF solvent model, however, charge scaling is less significant. Because of this, the charges are not scaled unless directly noted. The dipole moment $\vec{\mu}_{liq}$ in the liquid phase can be reduced as well and scales with $\vec{\mu}_s = \vec{\mu}_{liq}/n$, which we consider presently. 48

The dielectric theory of Onsager suggests that the intrinsic dipole moment $\overrightarrow{\mu}_0$ in the gas phase is shifted as $\overrightarrow{\mu}_{liq} = \overrightarrow{\mu}_0 + \alpha \overrightarrow{E}_R$ due to the reaction field \overrightarrow{E}_R exerted on the dipole in a hypothetical cavity situated in a dielectric medium with polarizability α . The $\alpha \overrightarrow{E}_R$ term indicates that the electric polarization at the location of the dipole $\overrightarrow{\mu}_0$ is instantaneously induced by the reaction field of the medium surrounding the dipole in the cavity. Thus, $\overrightarrow{\mu}_{liq}$ in a dielectric medium with a bulk dielectric constant ε_r and refractive index n can be calculated as follows:

$$\mu_{liq} = \frac{(2\varepsilon_r + 1)(n^2 + 2)\mu_0}{3(2\varepsilon_r + n^2)},$$
Eq. 5

where the non-vector symbols designate the magnitude of the corresponding vectors. This is used for the scaled dipole moment as shown above, $\mu_s = \mu_{liq}/n$.

For example, the values of μ_{liq} and μ_s for water are $\mu_{liq} = 2.31$ D and $\mu_s = 1.73$ D, respectively, when $\mu_0 = 1.85$ D, n = 1.33, and $\varepsilon_r = 78$. Nevertheless, Eq. 5 requires the bulk dielectric constant ε_r as an input, and this parameter may depend on other molecular or environmental parameters such as the temperature, molecular shape, and LJ parameter ε_{Ll} . However, for

polar solvents, $(2\varepsilon_r + 1)/(2\varepsilon_r + n^2)$ in Eq. 5 is approximately 1; therefore, the scaled dipole moment is mostly insensitive to changes in the dielectric constant ε_r . In the present study, we choose the dipole moment $\vec{\mu}$ in our simulations such that the calculated dielectric constant is consistent with the experimental value. We expect the chosen value to be comparable to the scaled dipole moment μ_s or unscaled dipole moment μ_{lia} . We consider this somewhat uncertain condition, allowing for flexibility in the SF model, because Eq. 5 and μ_s = μ_{liq}/n may not be completely accurate. For example, the calculated μ_{lia} value for MeOH is 2.10 D, whereas the experimental value is approximately 2.60-2.80 D.⁵⁰-53 Here, we note that our SF simulation method often overestimates the dielectric constant when the unscaled dipole moment μ_{liq} is used directly as a simulation input. This feature was discussed in the study of ellipsoidal SF fluids for organic solvents in Ref. 37, where introducing non-isotropic particle shapes can reduce the discrepancy between simulations and experiments. In this sense, dipole scaling could be regarded as a compensatory method for capturing the effects of particle anisotropy.

We perform MD simulations with the present model using LAMMPS.⁵⁴ We simulate the common polar solvents water, methanol, ethanol, acetone, 1-propanol, dimethylsulfoxide (DMSO), and dimethylformamide (DMF). Similar to the simulation in Ref. 36, the present simulations consist of boxes with side lengths of 21 Å for water and 30 Å for the other solvents. For the WCA potential, we use $\epsilon_{LJ}^{(water,water)} = 0.758$ kcal/mol, which we call parameter set 1. Parameter set 1 is applied to most of the solvents in Table 1 and is used in the sections on salt-free solvents, temperature dependence, and external field dependence on ε_r . 55, 56 For some simulations of water we use the LJ potential with $\epsilon_{\rm LI}^{({
m water,water})} = 0.36$ kcal/mol and a cutoff distance $r_c =$ 2.5σ , which we call parameter set 2. This parameter set is used in the sections on the temperature dependence of ε_r with NPT, external field dependence on ε_r , and NaCl solutions. Additional parameters beyond these parameter sets are noted in the relevant sections. The timestep is $\Delta t = 1$ fs. The simulations are equilibrated for $1 \times 10^6 - 2 \times 10^7$ timesteps (1–20 ns) at room temperature (300 K) using the Langevin thermostat, which includes the effects on the rotational degrees of freedom with a damping factor of $100\Delta t$, unless otherwise noted. The simulations were run to obtain more than 10000 samples by performing measurements every 5000 steps. The calculation of the dielectric constant of ion-containing water requires more than 20000 samples when the salt concentration becomes high, typically larger than 4 M. The Ewald summation

method for the electrostatic interactions is set to an accuracy of 10^{-6} .

B. Dielectric Constant Calculation

We calculate the dielectric constant according to the method proposed in Ref. 57. Note that the total dipole moment \vec{M}_{tot} of the system includes contributions from the permanent dipole moments of the charge-neutral solvents and the ionic charges of the salt ions. Thus, we write $\vec{M}_{tot} = \vec{M}_D + \vec{M}_J$, where $\vec{M}_D = \sum_i \vec{\mu}_i$ and $\vec{M}_J = \sum_i q_i \vec{r}_i$ designate the sum of the dipole moments $\vec{\mu}_i$ of each solvent particle and the dipole moment arising from the sum of the center of masses of the ionic charges, respectively. Note that when evaluating $\sum_i q_i \vec{r}_i$ the 'unwrapped' coordinates (the coordinates of the ions that have not been mapped back into the simulation box when an atom passes a periodic boundary) must be used. Given that $\langle \vec{M}_D \rangle = 0$ and $\langle \vec{M}_J \rangle = 0$ in isotropic systems, we calculate the dielectric constant as follows:

$$\begin{split} \varepsilon_r &= 1 + \frac{\left(\langle \vec{M}_{tot}^2 \rangle - \langle \vec{M}_{tot} \rangle^2\right)}{3V k_B T \varepsilon_0} \\ &= 1 + \frac{\left(\langle \vec{M}_D^2 \rangle + \langle \vec{M}_J^2 \rangle + 2 \langle \vec{M}_D \cdot \vec{M}_J \rangle\right)}{3V k_B T \varepsilon_0}. \end{split}$$
 Eq. 6

The latter two terms in the brackets represent the influence of ions on the dielectric constant. Without the effects of these ionic charges, Eq. 6 is reduced to

$$\varepsilon_r^{J=0} = 1 + \frac{\langle \vec{M}_D^2 \rangle}{3V k_B T \varepsilon_0}$$
 Eq. 7

We denote Eq. 7 as the "permanent dipole method."

To introduce the effects from the ionic charges we can use the EH method, 40, 41

$$\lim_{t \to \infty} \langle \Delta \vec{M}_J^2(t) \rangle = 6V k_B T \sigma(0) t + 2 \langle \vec{M}_J^2 \rangle, \qquad \text{Eq. 8}$$

where $\Delta \overrightarrow{M_J} \equiv \overrightarrow{M_J}(t) - \overrightarrow{M_J}(0)$ and $\sigma(0)$ is the static conductivity. Thus, the y-intercept of the linear behavior of $\langle \Delta \overrightarrow{M_J}^2(t) \rangle$ yields $\langle \overrightarrow{M_J}^2 \rangle$. It must be noted that the EH method is a diffusion method and requires $\overrightarrow{M_J}$ be calculated by the unwrapped positions of the particles. However, the cross term $\langle \overrightarrow{M_D} \cdot \overrightarrow{M_J} \rangle$ can use $\overrightarrow{M_J}$ calculated using wrapped coordinates due to translational symmetry arising from periodic boundary conditions. The effects of $\overrightarrow{M_J}$ and the dipole-charge coupling term $\overrightarrow{M_D} \cdot \overrightarrow{M_J}$ at high salt concentrations are complicated. These terms for ionic liquids tend to be comparable to the values of $\langle \overrightarrow{M_D}^2 \rangle$. However, we show in Section III that the coupling terms are negligible in

Table 1 Calculated dielectric constants ε_r of seven polar solvents with the WCA potential. μ , σ , ε_{LJ} , and number density are the input parameters for the simulations, whereas ε_r (exp) is the typical experimental value of the solvent dielectric constant. The solvent diameters σ are set to their typical experimental values. For comparison, we show the typical experimental values of μ_0 (exp) and the μ_{liq} and μ_s values calculated from Eq. 5. The refractive indices n are 1.33 (water and MeOH), 1.36 (EtOH and acetone), 1.38 (1-propanol and DMSO), and 1.43 (DMF). The number densities are the same as those used in our previous work.

5.0150), and 1.45 (Divit). The number defisities are the same as those used in our previous work.										
Mol / σ (Å)	μ (D)	$\mu_0(\exp)$ (D)	μ_{liq} (D)	μ_s (D)	$\epsilon_{\rm LJ}$ (kcal/mol)	$arepsilon_r$	$\varepsilon_r(\exp)$	Number Density (Å-3)		
Water / 2.8	1.75	1.85	2.31	1.74	0.758	85.7	78	0.03344		
Water / 2.8	1.73				0.758	81.7				
Water / 2.8	1.70				0.758	75.0				
MeOH / 4	2.25	1.69	2.10	1.58	0.758	32.4	33	0.01489		
MeOH / 4	2.02				0.758	30.2				
EtOH / 4.4	2.13	1.69	2.13	1.57	0.758	20.7	25.3	0.01152		
EtOH / 4.4	2.13				1.2	22.06				
Acetone / 4.6	2.66	2.88	3.62	2.66	0.758	23.9	20.7	0.00819		
Acetone / 4.6	2.66				0.1	19.7				
1-propanol / 4.9	2.14	1.68	2.14	1.55	0.758	10.5	20.1	0.00807		
1-propanol / 4.9	2.70				0.758	26.5				
1-propanol / 4.9	2.70				0.1	21.4				
DMSO / 4.53	3.70	3.96	5.11	3.70	0.758	212.2	47.2	0.00848		
DMSO / 4.53	3.70				0.05	100.5				
DMSO / 4.53	2.90				0.758	42.2				
DMSO / 4.53	3.00				0.758	47.0				
DMF / 4.72	3.00	3.86	5.13	3.59	0.758	37.8	36.7	0.00778		
DMF / 4.72	3.20				0.758	40.5				

NaCl solutions. As suggested by recent simulation studies of ionic liquids, ^{57, 59} the ionic contribution to the dielectric constant can be significant. We note that Eq. 6 accounts for the contribution from the dipole moment arising from ion-ion correlations such as ion pairs and ion clusters.

III. RESULTS

Salt-free solvents

Table 1 shows the simulated dielectric constants of seven polar solvents that best match the experimental value of ε_r . Each solvent species is labeled with respect to the corresponding molecular diameter. In this study, the dipole moment μ and LJ parameter ϵ_{LJ} (i.e., the strength of the repulsive force in the WCA potential) are adjustable input parameters in the simulations; however, ε_{LJ} is fixed at 0.758 kcal/mol for water. $^{55,\ 56}$ The densities used for the solvents are the same as the experimental values used in Ref. 36. As discussed in the previous section, we expect μ to be close to the scaled dipole moment μ_s ; otherwise, μ should fall in or near the range of μ_s to μ_{liq} . Given this guideline, the present results suggest that SFs can align with the seven types of solvents in terms of dielectric response because the calculated dielectric constants are comparable to the experimental values obtained at the corresponding molecular parameters. Nevertheless, caution must be taken when interpreting the consistency between simulation and experiment. First, as shown in the case of acetone and 1-propanol, a change in ϵ_{LI} can alter the calculated dielectric constant ε_r by up to 20%, which, while large, is not a drastic change. Second, the input dipole moment for 1-propanol should be larger than the dipole moment μ_0 in the gas phase and the dipole moment μ_{liq} in the liquid phase to reproduce the experimental dielectric constant $\varepsilon_r(\exp)$. In contrast, the dipole moments of DMSO and DMF must be smaller than the dipole moment μ_0 in the gas phase and scaled dipole moment μ_s . These differences could be attributed to asymmetry in the molecular shape³⁷ or the anisotropic charge distribution in the molecules, but the complete mechanism is unknown according to the current SF models because the differences could be reduced by optimizing a larger set of variables: the molecular diameter σ , LJ parameter ϵ_{LJ} , and dipole moment μ . We note that previous studies of the dipolar hard sphere Stockmayer fluid found that the dielectric constant is a function only of the dipole strength, a dimensionless quantity given by $\tilde{\mu}^2 = \mu^2/(kT\sigma^3)$. 60-62 We defer an investigation of similar scaling for the WCA Stockmayer fluid studied here to future work.

Temperature dependence of ε_r . We also consider the temperature dependence of the dielectric constant of

salt-free water. The black line representing $\mu = 1.73$ D with parameter set 1 in Fig. 1 shows that the SF model reasonably accounts for the changes in the dielectric constant of water as the temperature changes. The deviation from the experimental data increases as the temperature increases; however, this discrepancy is substantially improved when we set a linear dependence of the dipole moment $\mu = aT + b$ on the temperature in the simulation input. Fig. 1 shows the case with a and b such that $\mu = 1.73$ D and 1.85 D at T = 300 K and 370 K, respectively.

The temperature dependence of the refractive index n is small, and the dipole scaling method appears to be nearly independent of temperature. As discussed in the previous section, the term $(2\varepsilon_r + 1)/(2\varepsilon_r + n^2)$ in Eq. 5 is approximately 1, indicating that the temperature dependence of ε_r is unlikely to yield $\mu = \alpha T + b$. Thus, the temperature dependence of the dipole moment may be considered as an empirical model parameter. Otherwise, the hypothetical dipole scaling method could be modified to consider temperature dependence. Alternatively, we note that anisotropy in the particle shape may play an important role in reproducing the observed dielectric constant,³⁷ and thus, the steric effect decreases as the temperature increases. In this case, the temperature dependence of the dipole moment may be attributed to this change in the steric repulsion. The lack of the correct bond orientational order from hydrogen bonds could also cause the discrepancy between the simulation and experiment. However, we discuss in the next subsection that the current SF simulations appear to reasonably replicate the effect of the hydrogen bonds on the dielectric response of water.

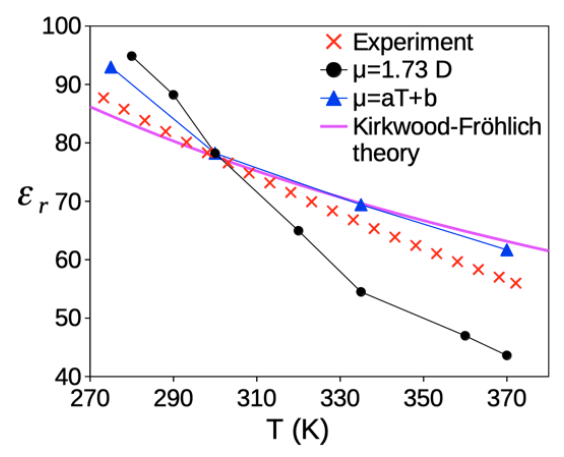


Fig. 1 Dielectric constant of salt-free water vs. temperature. The simulation results for the input parameter set with constant $\mu = 1.73$ D in Table 1 are shown as black circles. The solid lines for the simulation results are drawn to guide the reader. The experimental data reproduced from Ref. 63 are shown as red crosses. The simulation results obtained from the ansatz $\mu = aT + b$ are shown as blue triangles. The

coefficients a and b are set such that $\mu=1.73$ D and 1.85 D at T=300 K and 370 K, respectively. The purple solid line indicates the Kirkwood-Fröhlich equation.

For comparison, we also show the Kirkwood-Fröhlich theory (the standard equation for calculating the dielectric constant of polar liquids)

$$\frac{g\mu_0^2\rho}{9\varepsilon_0k_BT} = \frac{(\varepsilon_r - n^2)(2\varepsilon_r + n^2)}{\varepsilon_r(n^2 + 2)^2}$$
 Eq. 9

with g=2.80 and μ_0 =1.85 D for water in Fig. 1. Note that the dielectric constants obtained from standard force fields for atomistic water models, such as TIP4P/2005, TIP4Q, SPC/E, and SPC/ ε , also deviate from the experimental data.^{1, 2, 10} In this regard, the SF simulation result falls in the prediction range of these atomistic water models. Moreover, given that the recent OPC water model suggests the significance of the quadrupole moment in the temperature dependence of the dielectric constant,⁵ finely tuning the model parameters may require that the dipole-quadrupole and quadruple-quadrupole interactions be considered.

Parametrization with the NPT ensemble: Performing simulations at constant pressure requires the long-range attractive component of U_{LJ} in Eq. 1 to stabilize the liquid phases. Without the attractive part of the LJ potential, the current system cannot maintain a liquid phase at 1 atm.⁶⁴ Thus, we use parameter set 2 (i.e., $\epsilon_{LJ}^{(\text{water,water})} = 0.36 \text{ kcal/mol}$ and $r_c = 2.5\sigma$) for the LJ potential to reproduce the observed dielectric constant ($\epsilon_r = 78$) at 300 K and 1 atm, shown in Fig. 2. Moreover, this ϵ_{LJ} value leads to a density of 992 g/cm³, which is close to the observed value of 996 g/cm³ at 26 °C.⁶⁵

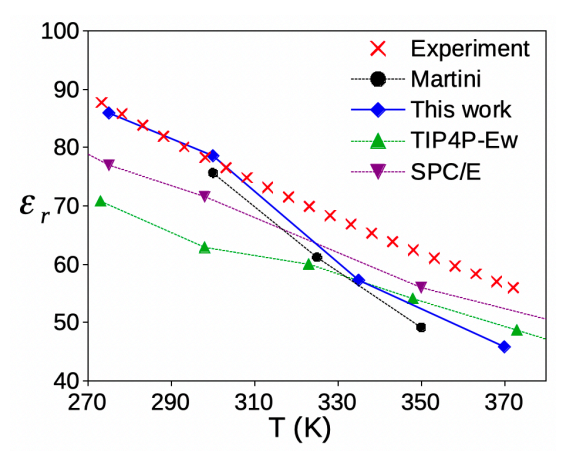


Fig. 2 Dielectric constant of salt-free water vs. temperature (the NPT ensemble). The simulation results obtained from the ansatz $\mu = aT + b$ with the same a and b values as in Fig. 1 are shown as blue triangles. The simulation results from the

polarizable MARTINI force field are shown as black circles, ⁵⁶ the TIP4P-Ew results are denoted as green triangles, and the SPC/E results are represented as purple upside-down triangles.

The simulation with $\mu=1.73$ D undergoes a liquid-vapor transition at temperatures lower than 370 K, and the simulation results underestimate the dielectric constant at high temperatures (e.g., $\varepsilon_r=45$ at 335 K). Thus, we invoke the temperature-dependent dipole moment $\mu=aT+b$, as determined from Fig. 1, instead of maintaining the constant dipole moment $\mu=1.73$ D in all temperature ranges. This yields a temperature-dependent dipole moment that is comparable to those of the polarizable MARTINI force field, ⁵⁶ TIP4P-Ew, ⁶⁶ and SPC/E. ⁶⁷ The model parameters could also be fine-tuned according to other thermodynamic properties (e.g., density and self-diffusion coefficient) by starting with the current parameter set.

External field dependence of \varepsilon_r. We also examine the dielectric response of salt-free water under strong electrostatic fields at room temperature (300 K). The significant decrease in the dielectric constant due to strong electrostatic fields may cause increases in electrostatic correlations. Here we use a modified version of Eq. 7 and calculate the field-dependent dielectric constant $\varepsilon_r = 1 + \langle M_z \rangle / (\varepsilon_0 VE)$ from the electric susceptibility $\langle M_z \rangle / (\varepsilon_0 VE)$ to an applied electrostatic field E, where $\langle M_z \rangle$ designates the average of the total dipole moment in the direction of the E field. Fig. 3 shows that the dielectric constant decreases as the electrostatic field increases. Our simulation results indicate no difference between using boxes with side lengths of 21 Å and 45 Å. For comparison, we calculated the dielectric constant using the Booth equation that accounts for the tetrahedral model for water and predicts changes in the dielectric constant as a function of external electrostatic fields.²² The Booth equation is given as

$$\begin{split} \varepsilon_r &= n^2 \\ &+ \frac{A\pi\rho(n^2+2)\mu_{th}}{E} L\left(\frac{B\mu_{th}(n^2+2)E}{kT}\right), \qquad \text{Eq. 9} \end{split}$$

where $A=28/(3\sqrt{78})$ and $B=\sqrt{73}$ /6 for the tetrahedral structure. $L(x)=\coth(x)-1/x$ is the Langevin function. We use the theoretical dipole moment $\mu_{th}=2.02$ D to reproduce the experimental dielectric constant $\varepsilon_r=78$, whereas Booth used $\mu_{th}=2.10$ D to reproduce $\varepsilon_r=80$. When the field is weak, the Booth equation is reduced to a formula analogous to the Kirkwood-Fröhlich equation. 68 Without the tetrahedral structure, the Booth equation in the limit of weak fields is reduced to the Onsager equation. Numerous theories and simulations have

invoked the Booth equation to analyze the field-dependent dielectric constant, including MD simulation for organic solvents, ⁶⁹ MD simulation for water confined between Pt slabs, ⁷⁰ and a modified Poisson-Boltzmann model for the bacterial porin OmpF. ⁷¹ Note that strong electric fields cause the dipoles to align in the field direction, thus reducing the fluctuation of the total dipole moment of the system. This effect causes the dielectric constant to decrease to a large degree, as indicated by Eq. 7. Thus, the qualitative agreement between the Booth equation and simulation result suggests that our water model based on SFs accounts for the correct dielectric response of water. Further finetuning of the model parameters appears to be required to improve the discrepancy between the two.

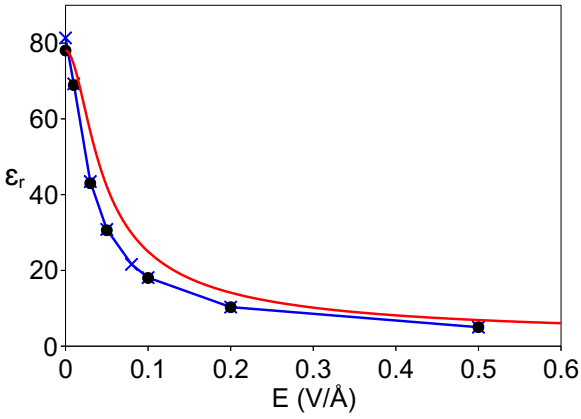


Fig. 3 Dielectric constants of water under electrostatic fields obtained from the simulation (black points for parameter set 2 and blue X dashed line for parameter set 1) and the Booth equation (red line).

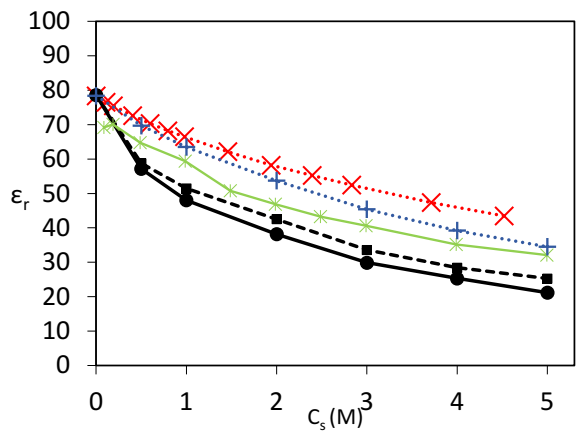


Fig. 4 Dielectric constant as a function of NaCl concentration. Experiment from Ref. 72 is shown in the red X dashed line and from Ref. 73 is shown in the blue + dashed line. Our results for permanent dipole method and EH method are the black circle solid line and black square dashed line, respectively. Green star solid line is the atomistic simulation result for the CC force field¹¹ which was reproduced from Ref. 10.

NaCl solutions

Next, we consider the addition of NaCl ions in water. We use parameter set 2 for $\epsilon_{LJ}^{(\text{water,water})}$, and include $\epsilon_{LJ}^{(+,+)} = \epsilon_{LJ}^{(-,-)} = \epsilon_{LJ}^{(\text{water,+})} = 0.1 \text{ kcal/mol}, \ \epsilon_{LJ}^{(\text{water,-})} = 3.0 \text{ kcal/mol}, \ \text{and} \ \epsilon_{LJ}^{(+,-)} = 0.07 \text{ kcal/mol}.$ For the salt ions, $\sigma_{Na}^{+} = 2.32 \text{ Å}, \ \sigma_{Cl}^{-} = 3.62 \text{ Å}$ with geometric mixing rules. The cutoffs are $r_c^{\mathrm{water}} = r_c^{\mathrm{(water,-)}} =$ 2.5σ , and $r_c = 2^{1/6}\sigma$ for all others. These parameters were selected to both match the dielectric constant $(\varepsilon_r=78)$ of unsalted water at 300 K and 1 atm and to prevent the formation of large, nearly immobilized ion clusters. Indeed, this type of cluster leads to phase separation between water and NaCl, thus we must avoid such an undesirable state. This salt-doped system should serve as a model system for examining the efficacy of our ion-containing SF fluid model because previous atomistic MD simulations, 10, 74-79 field-theoretical calculations,80 a hybrid of the Wertheim association model and Kirkwood-Fröhlich theory,23 and lattice Monte Carlo simulations with the field-dependent dielectric function⁸¹ have suggested that the strong electrostatic field arising from the ions saturates the molecular dipoles near the ions, and this effect significantly decreases the bulk dielectric constant. Intuitively, the cancellation of oppositely directed dipole moments²³ and the suppression of the dipoledipole correlation around the ions are the cause of this reduction in the dielectric constant. This polarization effect driven by the strong electrostatic field of the ions is referred to as dielectric saturation.

We first consider the contribution of the permanent dipole moment to the dielectric constant using the permanent dipole method (Eq. 7), shown in Fig. 4. The dielectric constant ε_r decreases consistently as the salt concentration c_s increases. The simulation results in Fig. 4 are consistent with the results of atomistic simulations using SPC/E with different ion force fields. 10 However, in contrast to the salt-free experimental value of 78 obtained at room temperature, the dielectric constants of salt-free water predicted by these atomistic simulations are 71.5 by the SPC/E atomistic simulation result closest to the experimental data in Fig. 4.10 It should be mentioned that some TIP4P models can more accurately predict the experimental dielectric constant of both salt-free and salt-containing water simulations. 76, 82

Table 2 Contributions of the permanent dipole moment (M_D) and collective translational dipole moment (M_J) with units $(e^2 Å^2)$ vs. the salt concentration c_s . $\varepsilon_r^{J=0}$ and ε_r^{EH} designate the dielectric constants calculated by the permanent dipole and EH methods, respectively.

c_s M	$\langle M_D^2 \rangle$	$\langle M_J^2 \rangle_{EH}$	$\langle M_D M_J \rangle$	$\varepsilon_r^{J=0}$	$arepsilon_r^{EH}$
0	308.07	0	0	78.60	78.60
0.5	223.15	6	0.06	57.21	60.26
1	186.84	12	0.74	48.06	54.23
2	147.45	17	0.18	38.14	46.54
3	114.81	15	-0.27	29.92	37.34
4	96.49	14	-0.84	25.30	31.93
5	80.18	14	1.09	21.20	28.55

We also consider the translational aspects of the ions and their effect on the dielectric constant through the EH (Eq. 8) method. Fig. 4 shows that this effect raises the dielectric constant of the system at concentrations greater than 1 M. While modest, this indicates that, at least in the case of the SF model, the influence of the ions on the dielectric constant should not be disregarded entirely. It must be noted, however, that in the EH method how one creates a linear fit can vary the y-intercept greatly, which consequently leads to a large uncertainty in $(\overrightarrow{M_J}^2)$. However, in the case of NaCl in water, the uncertainty in the fit is not large $(\pm 1 e^2 \mathring{A}^2)$. The results used for the calculations graphed in Fig. 4 are provided in Table 2.

We also compare this data with additional parameter sets, so we consider the effect of a scaled charge of q =0.85e on the dielectric constant, inspired by Ref. 83 and shown in Fig. 5, as well as a modified parameter set where $\epsilon_{L|}^{(\text{water},-)} = \epsilon_{L|}^{(\text{water},+)} = \epsilon_{L|}^{(+,-)} = \epsilon_{L|}^{(+,+)} =$ $\varepsilon_{\text{I},\text{I}}^{(-,-)} = \varepsilon_{\text{LI}}$ with a value of 0.1 or 0.01 kcal/mol with a cutoff of $r_c = 2^{1/6}\sigma$ and the bare electron charge q =1e, shown in Fig. 6. The dielectric constant arising from the permanent dipoles (Eq. 7) appears resistant to these changes in the parameter set, except in the case of ϵ_{LI} = 0.1 kcal/mol, though we still see a decrement in the dielectric constant as concentration increases. This indicates that the concentration of the ions is playing the dominant role and the exact nature of their interactions with the polar solvent is less so, the reason, however, is not immediately clear. In all cases the contribution to the dielectric constant from the ion translational motion as calculated with the EH method (Eq. 8) is small, except in the modified parameter set at high concentration, where we see an increase in ε_r^{EH} compared to $\varepsilon_r^{J=0}$. To probe further we examine NaCl pairs which can give us clues as to the differences of these parameter sets, and how they compare with experiment.

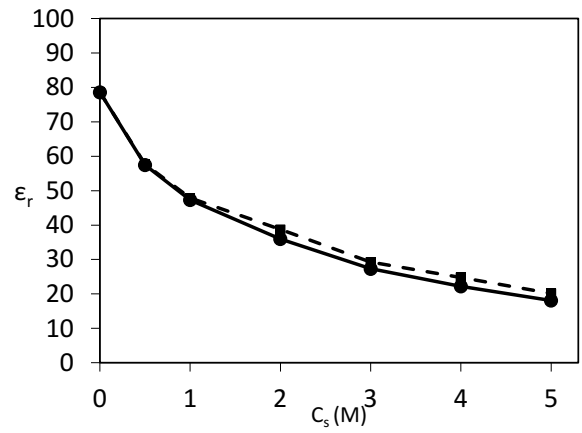


Fig. 5: Dielectric constant vs. NaCl concentration with a scaled charge of q = 0.85, parameter set 2 for $\epsilon_{\rm LJ}^{\rm (water,water)}$, and include $\epsilon_{\rm LJ}^{\rm (+,+)}=\epsilon_{\rm LJ}^{\rm (-,-)}=\epsilon_{\rm LJ}^{\rm (water,+)}=0.1$ kcal/mol, $\epsilon_{\rm LJ}^{\rm (water,-)}=3.0$ kcal/mol, and $\epsilon_{\rm LJ}^{\rm (+,-)}=0.07$ kcal/mol. For the salt ions, $\sigma_{Na^+}=2.32$ Å, $\sigma_{Cl^-}=3.62$ Å with geometric mixing rules. The cutoffs are $r_c^{\rm (water,water)}=r_c^{\rm (water,-)}=2.5\sigma$, and $r_c=2^{1/6}\sigma$ for all others. The results using the permanent dipole method and EH method are the black circle solid line and black square dashed line, respectively.

We analyze NaCl pairs using the radial distribution function,

$$g_{Na^+Cl^-}(r) = \frac{1}{4\pi r^2 \rho} \langle \sum_{i=1}^{Na^+} \sum_{j=1}^{Cl^-} \delta(|r_i - r_j| - r) \rangle$$
Eq. 10

and the coordination number

$$N_{NaCl}(r) = 4\pi \rho_{Na} + \int_0^r g_{Na} + c_l - (r')r'^2 dr'$$
 Eq. 11

comparing at several concentrations and using the parameter set from Fig. 4; results are shown in Fig. 7. All concentrations display high initial peaks, indicating ion pairing, but as concentration increases the peak decreases. Contrarily, coordination number increases with increasing concentration. At high concentrations (≥1M), ionic aggregates can form, with dipole moments smaller than isolated pairs, which could explain the small reduction in $\langle M_I^2 \rangle$ with increasing salt concentration above $c_s = 2M$. Diffraction experiments by Fuoss have indicated a lack of ion-pairing,8 but RDF's from atomistic simulations with favorable dielectric constants display ion pairs.84,10 More recent simulations and experiments also show increased clustering of ions at $c_s > 0.5$ M. 85-90 We note that the experimental analysis substantially depends on model parameters, such as the cutoff distance to define ion pairs and how the formation of ion clusters is treated. Moreover, another type of coarse-grained simulation, which is based on the mW water model, 91, 92 has been developed to mimic the tetrahedral coordination resulting from hydrogen bonds. This simulation accurately predicts the freezing point of water. The mW model shows a stronger ion pairing effect, which is consistent with our SFs. As a result, the dissimilarity between the atomistic and coarse-grained simulations RDF's may be attributed to the difference in the entropic effect that arises from ion pairing in the hydrogen-bonded network.

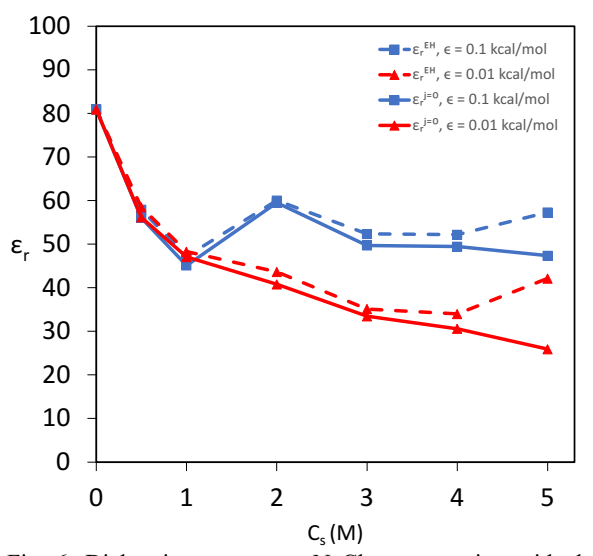


Fig. 6: Dielectric constant vs NaCl concentration with the modified parameter set $\epsilon_{\rm LJ}^{({\rm water},-)}=\epsilon_{\rm LJ}^{({\rm water},+)}=\epsilon_{\rm LJ}^{(+,-)}=\epsilon_{\rm LJ}^{(+,-)}=\epsilon_{\rm LJ}^{(-,-)}=\epsilon_{\rm LJ}$ with a cutoff of $r_c=2^{1/6}\sigma$ and the bare electron charge q=1e.

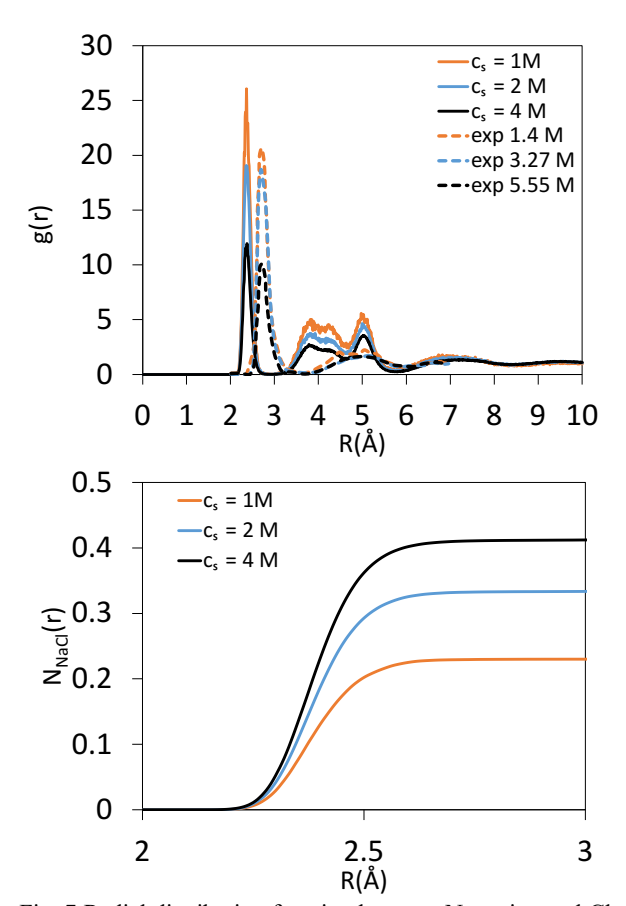


Fig. 7 Radial distribution function between Na cation and Cl anion at different concentrations with comparison to experiment from Ref. 85 (Top) and the corresponding coordination numbers, N_{NaCl}(r) (Bottom).

We remark that the prominent peak in the radial distribution function g(r) does not imply the presence of large ionic clusters. This observation is consistent with recent studies based on cluster analysis that utilized atomistic MD simulations with the SPC/E and TIP4P-Ew water models. 89, 90 To demonstrate this fact, we conducted a cluster analysis on the simulation results at different salt concentrations using an analysis tool in the software Ovito, 93 shown in Fig. 8. Defining a connection between two ions if their separation distance falls within a specified distance R_0 , a cluster consists of continuous connections between ions. Specifically, $R_0 = 2^{1/6}(\sigma_+ + \sigma_-)/2 = 3.33$ Å indicates that the cation and anion are in direct contact. Under these criteria, most clusters consist of one ion (a size of one). Moreover, when we consider more loosely connected clusters with $R_0 = 3.5$ Å, the clusters remain essentially the same, with very slight increases in the number of clusters with sizes 3 and 4. This indicates that a majority of ions exist as single particles or ion pairs, without forming substantial clusters. Remarkably, in the high salt concentration regime, this cluster ratio remains nearly unchanged.

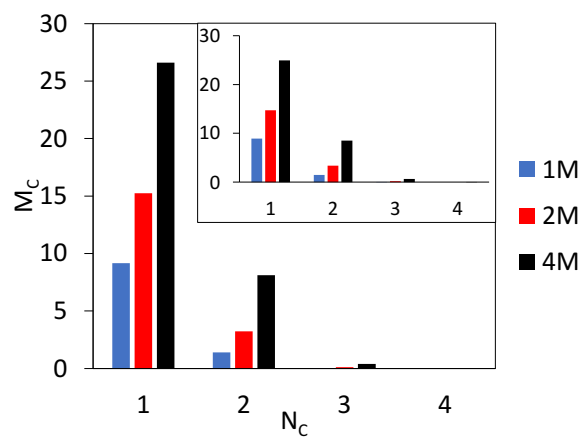


Fig. 8 The mean number of clusters, M_C , for each cluster size, N_C (number of ions in a cluster). Cluster cutoff distances, R_0 , compared are 3.33 Å and 3.5 Å (inset).

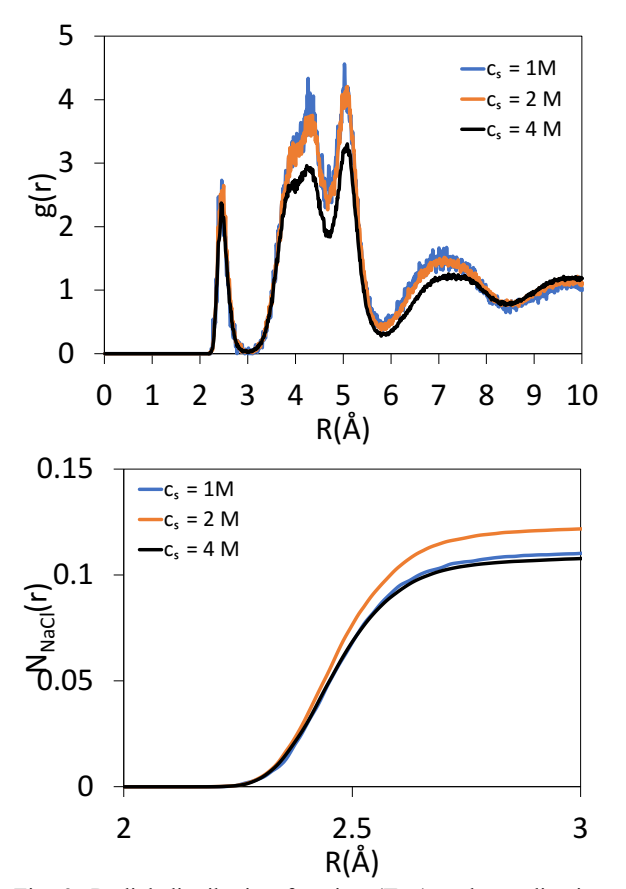


Fig. 9: Radial distribution function (Top) and coordination number (Bottom) between Na $^+$ and Cl $^-$ ions with a scaled charge of q=0.85e (same parameter set as Fig. 5) at various concentrations.

The radial distribution function and coordination numbers for the scaled charge system (q = 0.85e) shown in Fig. 9 have low first peaks (below 3)

indicating a distinct lack of any tightly bound NaCl pairs. This lack of pairs explains the less pronounced effect of the translation of the ions on the total dielectric constant, while still influencing the permanent dipoles. However, the alternative sets of modified parameters used in Fig. 6, applied to the unscaled charge (q = 1e), result in a qualitatively distinct scenario of ion clustering, as shown in Fig. 10 and Fig. 11. It is worth noting that the peak of the radial distribution function indicates substantial occurrences of ion pairing. As a result, the system exhibits an agglomeration of NaCl ions, not in a crystal structure, but rather as a large cluster of ions. This clustering structure is most pronounced at the highest concentration, where the separation in the dielectric constant occurs between the EH method and permanent dipole method. While these various parameter sets possess widely varied differences in ion dynamics, they result in very similar dielectric constants arising from permanent dipoles. Thus, we stress the importance of examining ion pairs and clusters in these systems to determine optimal parameters reflecting agreement with experiment.

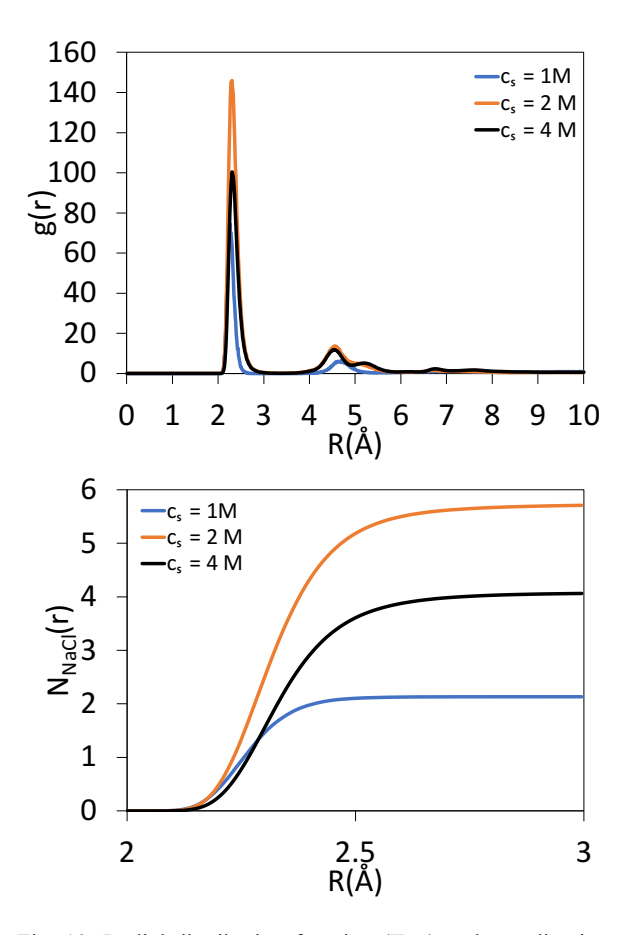


Fig. 10: Radial distribution function (Top) and coordination number (Bottom) between Na⁺ and Cl⁻ ions with $\epsilon_{LJ}=0.1$ kcal/mol, the same parameters as in Fig. 6. ($\epsilon_{LJ}^{(water,-)}=0.1$)

 $\epsilon_{\rm LJ}^{({\rm water},+)}=\epsilon_{\rm LJ}^{(+,-)}=\epsilon_{\rm LJ}^{(+,+)}=\epsilon_{\rm LJ}^{(-,-)}=\epsilon_{\rm LJ}$ with a cutoff of $r_c=2^{1/6}\sigma$ and the bare electron charge q=1e)

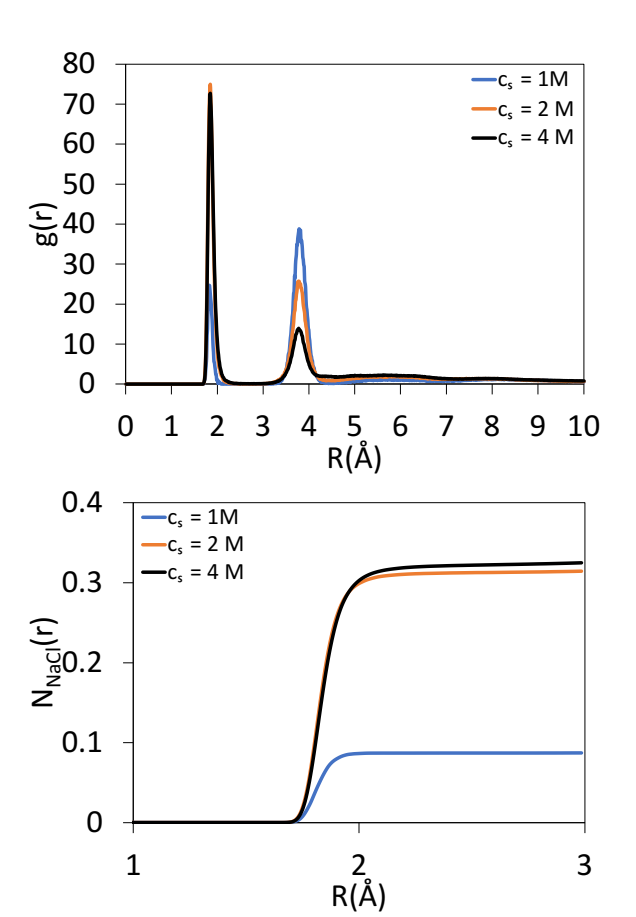


Fig. 11: Radial distribution function (Top) and coordination number (Bottom) between Na⁺ and Cl⁻ ions with $\epsilon_{LJ}=0.01$ kcal/mol, the same parameters as in Fig. 6. ($\epsilon_{LJ}^{(\text{water},-)}=\epsilon_{LJ}^{(\text{water},+)}=\epsilon_{LJ}^{(+,-)}=\epsilon_{LJ}^{(+,+)}=\epsilon_{LJ}^{(-,-)}=\epsilon_{LJ}$ with a cutoff of $r_c=2^{1/6}\sigma$ and the bare electron charge q=1e)

IV. CONCLUSION

We developed an SF model in Ref. 36 that accounts for the dielectric response of salt-free and salt-doped polar solvents. The aim of the current study is not to fine-tune the model parameters but to consider the practical applicability of the SF model in soft matter science. The SF model accounts for the dielectric constant of 7 polar solvents (water, MeOH, EtOH, acetone, 1-propanol, DMSO, and DMF). The temperature dependence of the dielectric constant of water in the simulation reproduces the trends in the experimental data and implies an ellipsoidal potential may be needed for more quantitative agreement. Calculations that include NaCl

ions find the dielectric constant of water decreases, which is consistent with experimental results. This saltinduced change in the dielectric constant arises mainly due to the dielectric saturation effect, which is consistent with previous results based on fieldtheoretical methods, 80 a hybrid of the Wertheim association model and Kirkwood-Fröhlich theory,²³ lattice-based simulations,81 and atomistic MD simulations. 10, 74, 75 The trend and magnitude of the dielectric decrement caused by the salt ions compare favorably with those obtained in previous atomistic MD simulations. Our simulations also show that the dielectric decrement is a robust characteristic dependent mainly on ion concentration, as different parameter sets displayed this qualitative behavior similarly. Thus, we emphasize the importance of examining ion pairs and clusters to determine appropriate parameters. Given the consistency in the ion solvation energies obtained in our previous work36 and dielectric constants of SF ellipsoidal solvents simulated by Johnson et al.,37 we conclude that the SF model can reasonably represent actual electrolytes using minimal sets of model parameters and degrees of freedom in terms of the Coulombic and dipolar electrostatic interactions. Thus, we suggest that the SF model is a computationally efficient and manageable approach that allows us to investigate systems and phenomena that pose greater computational challenges when using atomistic simulations.

ACKNOWLEDGMENTS

This material is based on work supported by the Faculty Early Career Development Program of the National Science Foundation under Grant DMR-1944211 and the Research Excellence Fund of Michigan Technological University under Grant REF-01634. This work was performed, in part, at the Center for Integrated Nanotechnologies, an Office of Science User Facility operated for the U.S. Department of Energy (DOE) Office of Science. Sandia National Laboratories is a multimission laboratory managed and operated by National Technology & Engineering Solutions of Sandia, LLC, a wholly owned subsidiary of Honeywell International, Inc., for the U.S. DOE's National Nuclear Security Administration under contract DE-NA-0003525. We are also grateful to the High-Performance Computing Shared Facility, Superior, at MTU for their essential support.

REFERENCES

¹ J. Alejandre *et al.*, Phys. Chem. Chem. Phys. **13** (2011) 19728.

- E. Meneses-Juarez, J. F. Rivas-Silva, and M. Gonzalez-Melchor, J. Phys.-Condes. Matter 30 (2018)
 M. W. Mahoney, and W. L. Jorgensen, J. Chem. Phys. 112 (2000) 8910.
- ⁴ J. G. Mendez-Bermudez *et al.*, J. Mol. Liq. **219** (2016) 354.
- ⁵ S. Izadi, R. Anandakrishnan, and A. V. Onufriev, J. Phys. Chem. Lett. **5** (2014) 3863.
- ⁶ L. P. Wang, T. J. Martinez, and V. S. Pande, J. Phys. Chem. Lett. **5** (2014) 1885.
- ⁷C. Vega *et al.*, Faraday Discuss **141** (2009) 251.
- ⁸ R. M. Fuoss, Proc. Natl. Acad. Sci. U. S. A. 77 (1980) 34.
- ⁹ E. Duboue-Dijon et al., J. Chem. Phys. **153** (2020)
- ¹⁰ S. Seal, K. Doblhoff-Dier, and J. Meyer, J. Phys. Chem. B **123** (2019) 9912.
- ¹¹ S. Chowdhuri, and A. Chandra, J. Chem. Phys. **115** (2001) 3732.
- ¹² C. Schroder *et al.*, J. Chem. Phys. **140** (2014)
- ¹³ O. Steinhauser et al., J. Chem. Phys. **129** (2008)
- ¹⁴ P. Loche et al., J. Phys. Chem. B **125** (2021) 8581.
- ¹⁵ V. S. Kuznetsov, N. V. Usol'tseva, and V. P. Zherdev, Russ J Inorg Chem+ **59** (2014) 637.
- ¹⁶ O. Y. Samoilov, *Structure of Aqueous Electrolyte Solutions and the Hydration of Ions* (Consultants Bureau, 1965), 185.
- ¹⁷ H. Sirringhaus *et al.*, Advanced Materials **22** (2010) 3893.
- ¹⁸ J. Gavis, Chem. Eng. Sci. **19** (1964) 237.
- ¹⁹ W. R. Fawcett, and A. C. Tikanen, J. Phys. Chem. **100** (1996) 4251.
- ²⁰ J. G. Kirkwood, J. Chem. Phys. **7** (1939) 911.
- ²¹ U. H. Choi et al., Macromolecules **46** (2013) 1175.
- ²² F. Booth, J. Chem. Phys. **19** (1951) 391.
- ²³ B. Maribo-Mogensen, G. M. Kontogeorgis, and K. Thomsen, J. Phys. Chem. B **117** (2013) 10523.
- ²⁴ C. Kriebel, and J. Winkelmann, Mol. Phys. **88** (1996) 559.
- ²⁵ R. Hentschke, J. Bartke, and F. Pesth, Phys. Rev. E **75** (2007)
- ²⁶ S. Goldman, Mol. Phys. **71** (1990) 491.
- ²⁷ E. L. Pollock, and B. J. Alder, Physica A **102** (1980)
- ²⁸ F. J. Vesely, Chem. Phys. Lett. **56** (1978) 390.
- ²⁹ S. G. Moore, M. J. Stevens, and G. S. Grest, Phys. Rev. E **91** (2015)
- ³⁰ M. J. Stevens, and G. S. Grest, Phys. Rev. E **51** (1995) 5976.
- ³¹ S. Paul, and A. Chandra, J. Phys. Chem. B **107** (2003) 12705.
- ³² K. Kiyohara, K. E. Gubbins, and A. Z. Panagiotopoulos, J. Chem. Phys. **106** (1997) 3338.
- ³³ J. Bartke, and R. Hentschke, Phys. Rev. E **75** (2007)
- ³⁴ G. T. Gao, X. C. Zeng, and W. C. Wang, J. Chem. Phys. **106** (1997) 3311.
- ³⁵ V. A. Payne *et al.*, J. Phys. Chem. **97** (1993) 10478.

- ³⁶ C. J. Shock et al., J Phys Chem B **124** (2020) 4598.
- ³⁷ L. E. Johnson *et al.*, J. Phys. Chem. B **114** (2010) 8431.
- ³⁸ L. Perera, and M. L. Berkowitz, J. Chem. Phys. **96** (1992) 3092.
- ³⁹ A. Chandra, J. Chem. Phys. **113** (2000) 903.
- ⁴⁰C. Schroder, M. Haberler, and O. Steinhauser, J Chem Phys **128** (2008) 134501.
- ⁴¹ E. Helfand, Phys. Rev. **119** (1960) 1.
- ⁴² T. Gao et al., MRS Communications (2022)
- ⁴³ I. V. Leontyev et al., J. Chem. Phys. **119** (2003) 8024.
- ⁴⁴ I. V. Leontyev, and A. A. Stuchebrukhov, J. Chem. Phys. **130** (2009)
- ⁴⁵ I. Leontyev, and A. Stuchebrukhov, Phys. Chem. Chem. Phys. **13** (2011) 2613.
- ⁴⁶ C. Schröder, Phys. Chem. Chem. Phys. **14** (2012) 3089.
- ⁴⁷ C. Schröder, A. Lyons, and S. W. Rick, Phys. Chem. Chem. Phys. **22** (2020) 467.
- ⁴⁸ A. Farahvash, I. Leontyev, and A. Stuchebrukhov, J. Phys. Chem. A **122** (2018) 9243.
- ⁴⁹ G. G. Raju, *Dielectrics in electric fields* (CRC Press, Taylor & Francis Group, 2016), 2nd edn.,
- ⁵⁰ T. Ishiyama, V. V. Sokolov, and A. Morita, J. Chem. Phys. **134** (2011)
- ⁵¹ N. Sieffert *et al.*, J Chem Theory Comput **9** (2013) 106
- ⁵² M. Jorge, J. R. B. Gomes, and M. C. Barrera, J. Mol. Liq. **356** (2022)
- ⁵³ A. L. McClellan, *Tables of experimental dipole moments* (W.H. Freeman, San Francisco, 1963),
- ⁵⁴ S. Plimpton, J. Comput. Phys. **117** (1995) 1.
- ⁵⁵C. Herdes, T. S. Totton, and E. A. Muller, Fluid Phase Equilibr **406** (2015) 91.
- ⁵⁶ S. O. Yesylevskyy *et al.*, Plos Comput Biol **6** (2010)
- ⁵⁷ C. Schroder, and O. Steinhauser, in *Computational spectroscopy: methods, experiments and applications* (Wiley-VCH, Weinheim, 2010), p. 279.
- ⁵⁸ F. Dommert *et al.*, J. Chem. Phys. **129** (2008)
- ⁵⁹ C. Schröder *et al.*, The Journal of chemical physics **127** (2007) 044505.
- ⁶⁰ S. Kournopoulos *et al.*, The Journal of Chemical Physics **156** (2022) 154111.
- ⁶¹L. Neumaier *et al.*, Fluid Phase Equilibria **555** (2022) 113346.
- ⁶² M. Kohns, J. Marx, and K. Langenbach, Chemical Engineering Science **245** (2021) 116875.
- ⁶³ C. G. Malmberg, and A. A. Maryott, Journal of Research of the National Bureau of Standards **56** (1956) 2641
- ⁶⁴ M. Van Leeuwen, and B. Smit, Physical review letters **71** (1993) 3991.
- ⁶⁵ J. R. Rumble, D. R. Lide, and T. J. Bruno, *CRC Handbook of Chemistry and Physics* (CRC Press, Taylor & Francis Group, 2019), 100th edn.,
- ⁶⁶ H. W. Horn et al., J. Chem. Phys. **120** (2004) 9665.

- ⁶⁷ N. J. English, Mol. Phys. **103** (2005) 1945.
- ⁶⁸ H. Chen, and I. Nakamura, J. Phys. Chem. C **119** (2015) 24714.
- ⁶⁹ I. N. Daniels, Z. X. Wang, and B. B. Laird, J. Phys. Chem. C **121** (2017) 1025.
- ⁷⁰ I. C. Yeh, and M. L. Berkowitz, J. Chem. Phys. **110** (1999) 7935.
- ⁷¹ M. Aguilella-Arzo *et al.*, Phys. Chem. Chem. Phys. **11** (2009) 358.
- ⁷² R. Buchner, G. T. Hefter, and P. M. May, J. Phys. Chem. A **103** (1999) 1.
- ⁷³ V. Shcherbakov, Y. M. Artemkina, and E. Korotkova, Russian Journal of Inorganic Chemistry **59** (2014) 922.
- ⁷⁴ C. S. Babu, and C. Lim, J. Phys. Chem. B **103** (1999) 7958.
- ⁷⁵ C. S. Babu, and C. Lim, Chem. Phys. Lett. **310** (1999) 225.
- ⁷⁶ R. Fuentes-Azcatl, and M. C. Barbosa, The Journal of Physical Chemistry B **120** (2016) 2460.
- ⁷⁷ I. Zeron, J. Abascal, and C. Vega, The Journal of chemical physics **151** (2019) 134504.
- ⁷⁸ I. Pethes, Journal of Molecular Liquids **242** (2017) 845.
- ⁷⁹ D. Pache, and R. Schmid, ChemElectroChem 5 (2018) 1444
- ⁸⁰ A. Levy, D. Andelman, and H. Orland, Phys. Rev. Lett. **108** (2012) 227801.
- ⁸¹ X. Z. Duan, and I. Nakamura, Soft Matter **11** (2015) 3566.
- ⁸² D. Saric, M. Kohns, and J. Vrabec, The Journal of Chemical Physics **152** (2020) 164502.
- ⁸³ R. C. DeMille, and V. Molinero, The Journal of chemical physics **131** (2009) 034107.
- ⁸⁴ J. Sala, E. Guardia, and J. Marti, The Journal of chemical physics **132** (2010) 214505.
- ⁸⁵ R. Mancinelli *et al.*, The Journal of Physical Chemistry B **111** (2007) 13570.
- ⁸⁶ H. Bian *et al.*, Proceedings of the National Academy of Sciences **108** (2011) 4737.
- ⁸⁷ S. A. Hassan, The Journal of Physical Chemistry B **112** (2008) 10573.
- ⁸⁸ A. A. Chen, and R. V. Pappu, The Journal of Physical Chemistry B **111** (2007) 6469.
- ⁸⁹ D. Schaefer, and M. Kohns, Fluid Phase Equilibria **571** (2023) 113802.
- ⁹⁰ A. Benavides *et al.*, Molecular Physics **115** (2017) 1301.
- ⁹¹ R. C. DeMille, and V. Molinero, J. Chem. Phys. **131** (2009)
- ⁹² V. Molinero, and E. B. Moore, The Journal of Physical Chemistry B **113** (2009) 4008.
- ⁹³ A. Stukowski, Modelling and simulation in materials science and engineering **18** (2009) 015012.